Potassium 5p Line Data

David McKay

(Dated: June 2009 v1.0)

Contents

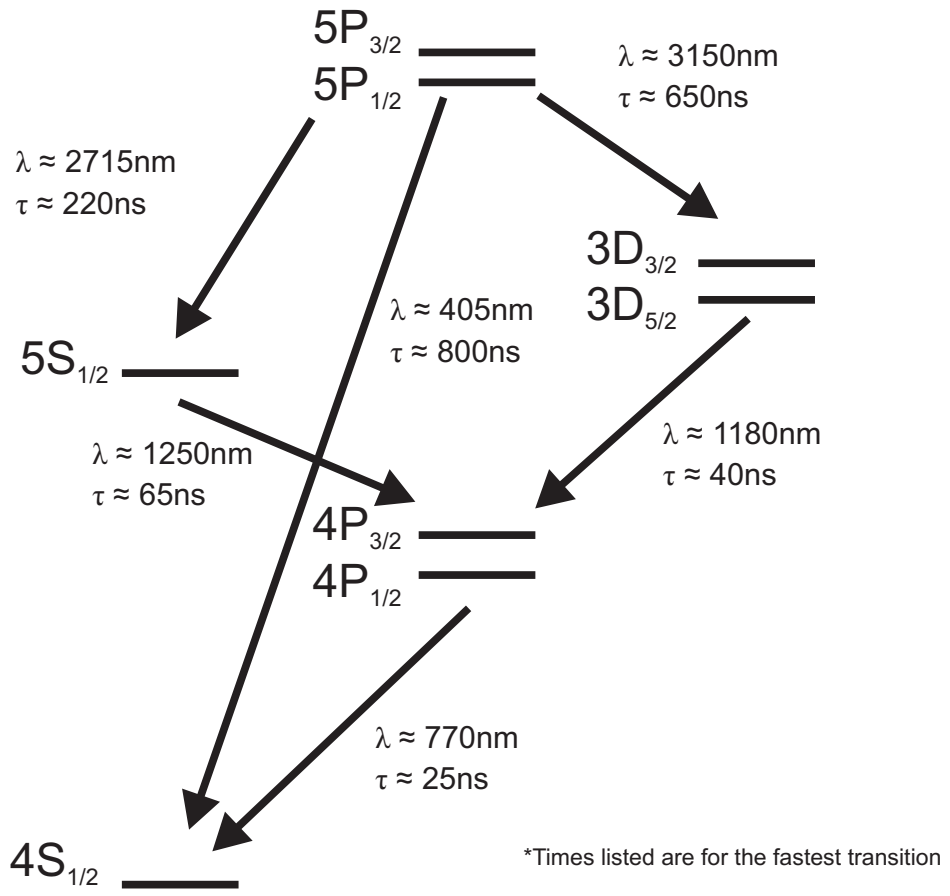

FIG. 1: Energy levels associated with decay from the $5p$ state of K. Rough values of the wavelength and decay between states are listed.

I. INTRODUCTION

This document is intended to be a list of the relevant properties of ^{39}K and ^{40}K when exciting the $4s \rightarrow 5p$ transition as motivated by similar documents for ^{87}Rb [21] and ^{40}K [14] for the $4s \rightarrow 4p$ transition. Since the $5p$ level is not the first excited state, information on a number of lines is required because there are several decay paths back to the ground state. All the levels associated with decay from the $5p$ state are illustrated in Figure 1.

The remaining part of this section will summarize some of the equations used in subsequent sections to calculate atomic properties from experimental data. In addition, Table I lists relevant physical constants that will be used throughout this document. Section II will list in more detail the transition properties (i.e. frequency and decay time) between the various levels. Section III will discuss the more detailed hyperfine structure of each

Speed of Light	c	2.99792458×10^8 m/s	[16]
Atomic Mass Unit	u	$1.660538782(83) \times 10^{-27}$ kg	[16]
Plank's Constant	$\hbar$	$1.054571628(53) \times 10^{-34}$Js	[16]
Vacuum Permittivity	ϵ_0	$8.854187817 \times 10^{-12}$F/m	[16]
Mass of ^{39}K	m_{39}	64.761×10^{-27} kg	
Mass of ^{40}K	m_{40}	66.422×10^{-27} kg	
Nuclear Spin of ^{39}K	I	3/2	[12]
Nuclear Spin of ^{40}K	I	4	[12]

TABLE I: Fundamental Constants and K Properties

level. Finally, Section IV will concern properties of the driven $5p$ transition, such as the cross-section, saturation intensity and branching ratios.

A. Reduced Dipole Matrix Elements

The following is a summary on reduced dipole matrix elements for optical transitions and how they relate to decay times and to Rabi rates between specific m_F levels. The decay rate A_{fi} between levels $|f\rangle$ and $|i\rangle$ is related to the matrix element between those states by the expression,

$$A_{ki} = \frac{\omega_0^3}{3\pi\epsilon_0\hbar c^3} \sum_q \left| \langle f | \, er_q^{(1)} \, | i \rangle \right|^2$$

where the sum q is over all outgoing polarizations. However, the decay rate is usually quoted between J levels and then we have to average over the m_J levels in the upper state and sum over the m_J levels in the lower state. The final result is that the decay rate from $J \to J'$,

$$A_{JJ'} = \frac{\omega_0^3}{3\pi\epsilon_0\hbar c^3} \frac{| \langle nJ | \, |er| \, | n'J' \rangle |^2}{2J+1} \tag{1}$$

where $\langle nJ||d||n'J'\rangle$ is the reduced dipole matrix element in units of Coloumb meter. This is often the decay rate that is measured. However, we may want to relate this decay rate to

the decay rate between hyperfine levels. The decay from $|JFm_F\rangle \rightarrow |J'F'm'_F\rangle$ for an atom with nuclear spin I is,

$$\begin{aligned} A_{Fm_F,F'm'_F} &= \frac{\omega_0^3}{3\pi\epsilon_0\hbar c^3}\sum_q \begin{pmatrix} F & 1 & F' \\ -m_F & q & m'_F \end{pmatrix}^2 |\langle nJF||er||n'J'F'\rangle|^2 \\ &= \frac{\omega_0^3}{3\pi\epsilon_0\hbar c^3}\sum_q \begin{pmatrix} F & 1 & F' \\ -m_F & q & m'_F \end{pmatrix}^2 (2F'+1)(2F+1)\begin{Bmatrix} J & F & I \\ F' & J' & 1 \end{Bmatrix}^2 |\langle nJ||er||n'J'\rangle|^2 \end{aligned}$$

where () are Wigner 3-j symbols and {} are Wigner 6-j symbols. Note that the conventions of [13] are used for these symbols. For the decay from $F \rightarrow F'$ (averaged over all m_F levels and summing over m'_F),

$$\begin{aligned} A_{FF'} &= \frac{\omega_0^3}{3\pi\epsilon_0\hbar c^3}(2F'+1)\begin{Bmatrix} J & F & I \\ F' & J' & 1 \end{Bmatrix}^2 |\langle nJ||er||n'J'\rangle|^2 \\ &= (2F'+1)(2J+1)\begin{Bmatrix} J & F & I \\ F' & J' & 1 \end{Bmatrix}^2 A_{JJ'} \end{aligned}$$

Note that the Rabi rate can be related to the decay rate by these reduced dipole matrix elements. The Rabi rate driving from $|JFm_F\rangle \rightarrow |J'F'm'_F\rangle$ with $\hat{\epsilon}$ polarized light is,

$$\begin{aligned} |\Omega|^2 &= \left(\frac{2I}{\hbar^2\epsilon_0 c}\right)\left|\sum_q \hat{\epsilon}\cdot\hat{\epsilon}_q \begin{pmatrix} F & 1 & F' \\ -m_F & q & m'_F \end{pmatrix}\right|^2 (2F+1)(2F'+1)\begin{Bmatrix} J & F & I \\ F' & J' & 1 \end{Bmatrix}^2 |\langle nJ||er||n'J'\rangle|^2 \\ &= \left(\frac{6\pi c^2 A_{JJ'} I}{\hbar\omega_0^3}\right)\left|\sum_q \hat{\epsilon}\cdot\hat{\epsilon}_q \begin{pmatrix} F & 1 & F' \\ -m_F & q & m'_F \end{pmatrix}\right|^2 (2J'+1)(2F+1)(2F'+1)\begin{Bmatrix} J & F & I \\ F' & J' & 1 \end{Bmatrix}^2 \end{aligned}$$

B. Hyperfine Structure

The magnetic dipole and electric quadrupole parts of the hyperfine interaction are characterized, respectively, by the constants A and B. The energy shift for a state with total electronic angular momentum J, nuclear angular momentum I and total angular momentum F ($F = J + I$), as a function of A and B, is

$$\Delta E \;=\; \frac{1}{2}AK + \frac{B}{4}\left(\frac{3K(K+1) - 4I(I+1)J(J+1)}{2I(2I-1)J(2J-1)}\right) \tag{2}$$

where $K = F(F+1) - I(I+1) - J(J+1)$.

C. G Factors

In the low-field limit, the magnetic field splitting is given by

$$\Delta E \;=\; \mu_B g_F m_F |B|$$

where,

$$\begin{aligned} g_F &= g_J \frac{F(F+1) - J(J+1) - I(I+1)}{2F(F+1)}, \\ g_J &= \frac{3}{2} + \frac{S(S+1) - L(L+1)}{2J(J+1)}. \end{aligned}$$

If we want to solve for the high-field limit we can no longer use $\mathbf{F}$ as a good quantum number and we must diagonalize the Hamiltonian,

$$\mathbf{H} \;=\; \mathbf{H}_{hf}(\mathbf{I}\cdot\mathbf{J}) + \mu_B g_J m_J |B|,$$

using the basis states $|I, m_I, J, m_J\rangle$. If the Zeeman term is much larger than the hyperfine term than the states $|I, m_I, J, m_J\rangle$ are eigenstates and we can solve for the hyperfine energy as a perturbation, $\langle I, m_I, J, m_J|\mathbf{H}_{hf}|I, m_I, J, m_J\rangle$.

II. TRANSITION PROPERTIES

In the following section we will list detailed properties of each of the optical transitions from Figure 1. While most of the data here is from [19], similar data can be found from [17], however, [19] uses newer references for all but the $4S \rightarrow 5P$ wavelength. All the following transition frequencies are assumed to be hyperfine free. Therefore, the hyperfine shift (Equation 2) is with respect to these frequencies.

A. $4S \rightarrow 4P$ (D1 and D2) transitions

The following is data for the $4S \rightarrow 4P$ transitions. The most recent measurement appears to be [10]. They measure the D1 and D2 lines of both ^{39}K and ^{40}K using a frequency comb. This data is used in the collection of K spectra by [19]. The isotope shift for the D transitions are obtained by subtracting the D1 lines for ^{39}K and ^{40}K . We can see that the isotope shift is mostly accounted for by the normal mass shift,

$$\delta\nu \;=\; \nu_{39}\left(1 - \frac{40}{39}\frac{m_e + m_{39}}{m_e + m_{40}}\right)$$

which is ~ -135MHz for the D transitions compared to the actual value of -125MHz. As noted in [7] the specific mass shift and the volume shift for the D transitions between ^{39}K and ^{40}K is -10.79(0.26)MHz for the D1 line and -10.55(0.30)MHz for the D2 line. Since these are less than 10% of the measured effect, a good approximation for the ^{40}K lines for the other transitions will be to use the normal mass shift. Another good reference is [12].

Frequency	ν	391016.17003(12) GHz	[10]
Wavelength (Vacuum)	λ	766.7009 nm	[1]
Transition Probability	A_{ki}	$3.80 \times 10^7 s^{-1}$	[19]
Decay Rate	$1/A_{ki}$	26.34(5)ns	[22]
Reduced Dipole Matrix Element	$\langle i\|d\|j\rangle$	1.23×10^{-29}Cm	[2]

TABLE II: $4S_{1/2} \rightarrow 4P_{3/2}$ (D2) transition properties for ^{39}K

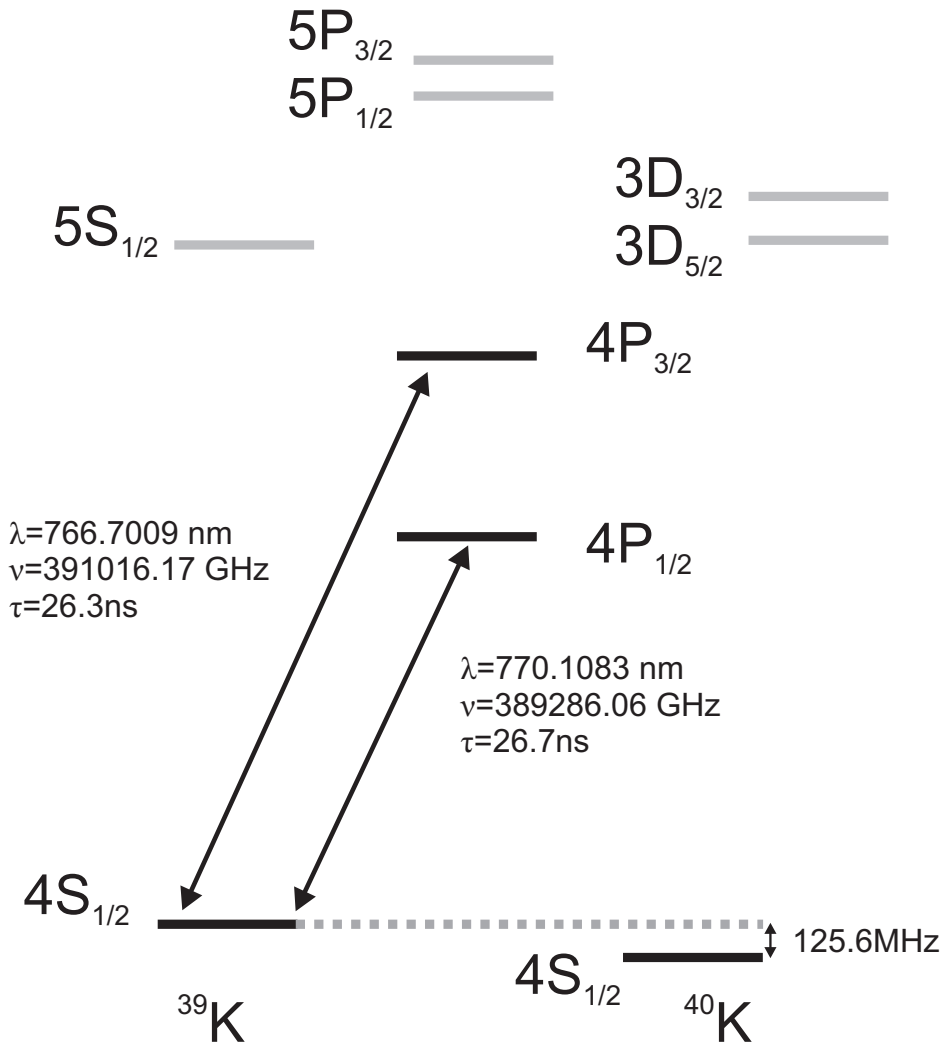

FIG. 2: $4S \rightarrow 4P$ transitions (D1 and D2) for ^{39}K with the isotope shift for ^{40}K indicated. Data from [19].

Frequency	ν	389286.058716(62) GHz	[10]
Wavelength (Vacuum)	λ	770.1084 nm	[1]
Transition Probability	A_{ki}	$3.75 \times 10^7 s^{-1}$	[19]
Decay Rate	$1/A_{ki}$	26.69(5)ns	[22]
Reduced Dipole Matrix Element	$\langle i\|d\|j\rangle$	1.74×10^{-29}Cm	[2]

TABLE III: $4S_{1/2} \rightarrow 4P_{1/2}$ (D1) transition properties for ^{39}K

Frequency	ν	391016.296050(88) GHz	[10]
Wavelength (Vacuum)	λ	766.7007 nm	[1]

TABLE IV: $4S_{1/2} \rightarrow 4P_{3/2}$ (D2) transition properties for ^{40}K

Frequency	ν	389286.184353(73) GHz	[10]
Wavelength (Vacuum)	λ	770.1081 nm	[1]

TABLE V: $4S_{1/2} \rightarrow 4P_{1/2}$ (D1) transition properties for ^{40}K

B. $4S \rightarrow 5P$

This data is mostly from [17] and [19]. [17] has more recent values for the wavelength, but [19] has more recent values for A_{ki}. Here the isotope shift is estimated from the normal mass shift and must be taken as approximate.

Frequency	ν	441091.07 GHz	[3]
Wavelength (Vacuum)	λ	404.5285 nm	[17]
Transition Probability	A_{ki}	$1.16 \times 10^6 s^{-1}$	[19]
Decay Rate	$1/A_{ki}$	862ns	[4]
Reduced Dipole Matrix Element	$\langle i\|d\|j\rangle$	8.25×10^{-31}Cm	[2]

TABLE VI: $4S_{1/2} \rightarrow 5P_{3/2}$ transition properties for ^{39}K

Frequency	ν	740528.89 GHz	[3]
Wavelength (Vacuum)	λ	404.8356 nm	[17]
Transition Probability	A_{ki}	$1.07 \times 10^6 s^{-1}$	[19]
Decay Rate	$1/A_{ki}$	935ns	[4]
Reduced Dipole Matrix Element	$\langle i\|d\|j\rangle$	1.12×10^{-30}Cm	[2]

TABLE VII: $4S_{1/2} \rightarrow 5P_{1/2}$ transition properties for ^{39}K

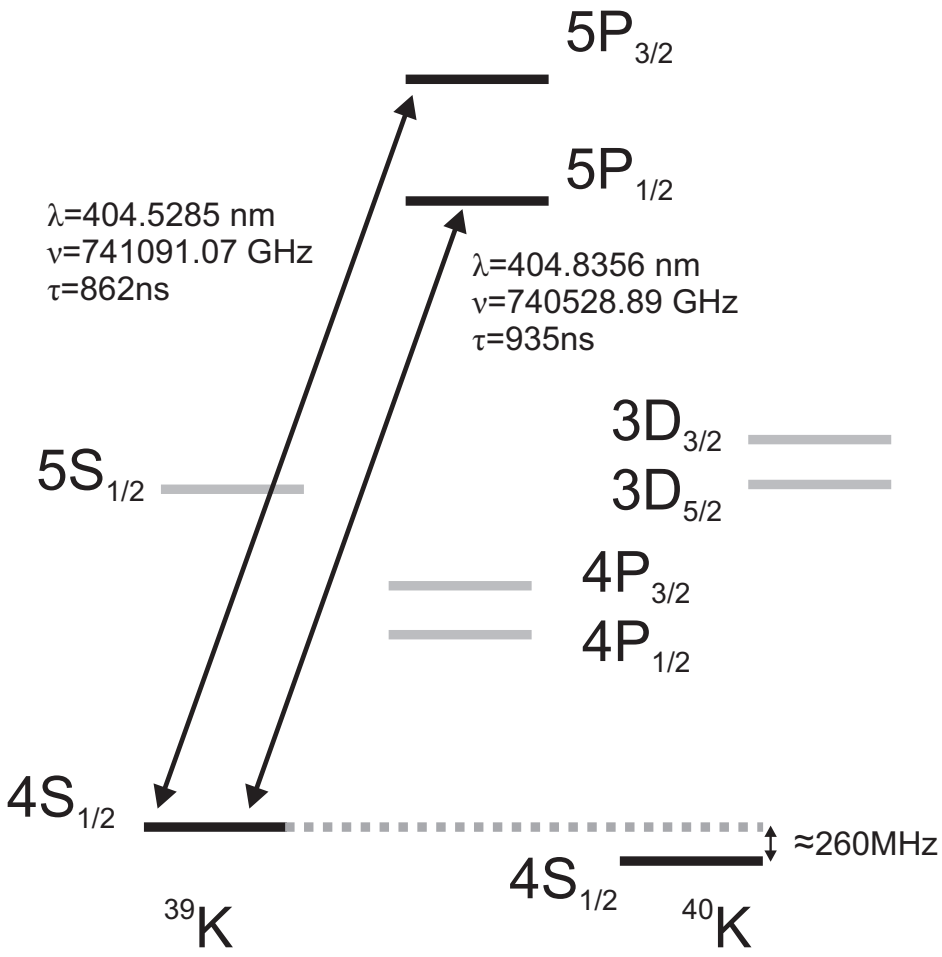

FIG. 3: $4S \rightarrow 5P$ transitions for ^{39}K with the isotope shift for ^{40}K indicated. Data from [19] and [17].

Frequency	ν	741091.33 GHz	[5]
Wavelength (Vacuum)	λ	404.5284 nm	[1]

TABLE VIII: $4S_{1/2} \rightarrow 5P_{3/2}$ transition properties for ^{40}K

Frequency	ν	740529.15 GHz	[5]
Wavelength (Vacuum)	λ	404.8355 nm	[1]

TABLE IX: $4S_{1/2} \rightarrow 5P_{1/2}$ transition properties for ^{40}K

C. $4P \rightarrow 5S$

This data is from [19]. Here the isotope shift is estimated from the normal mass shift and must be taken as approximate.

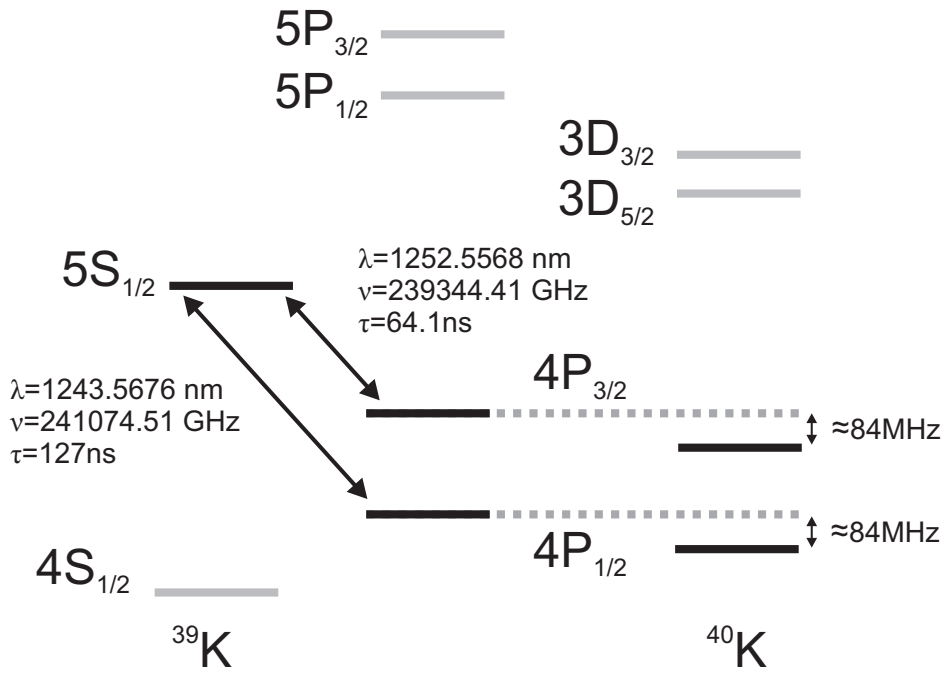

FIG. 4: $4P \rightarrow 5S$ transitions for ^{39}K with the isotope shift for ^{40}K indicated. Data from [19].

Frequency	ν	241074.51 GHz	[19]
Wavelength (Vacuum)	λ	1243.5676 nm	[1]
Transition Probability	A_{ki}	$7.9 \times 10^6 s^{-1}$	[19]
Decay Rate	$1/A_{ki}$	127ns	[4]
Reduced Dipole Matrix Element	$\langle i\|d\|j\rangle$	1.64×10^{-29}Cm	[2]

TABLE X: $4P_{1/2} \rightarrow 5S_{1/2}$ transition properties for ^{39}K

Frequency	ν	239344.41 GHz	[19]
Wavelength (Vacuum)	λ	1252.5568 nm	[1]
Transition Probability	A_{ki}	$1.56 \times 10^7 s^{-1}$	[19]
Decay Rate	$1/A_{ki}$	64.1ns	[4]
Reduced Dipole Matrix Element	$\langle i\|d\|j\rangle$	2.33×10^{-29}Cm	[2]

TABLE XI: $4P_{3/2} \rightarrow 5S_{1/2}$ transition properties for ^{39}K

Frequency	ν	241074.59 GHz	[5]
Wavelength (Vacuum)	λ	1243.569 nm	[1]

TABLE XII: $4P_{1/2} \rightarrow 5S_{1/2}$ transition properties for ^{40}K

Frequency	ν	239344.49 GHz	[5]
Wavelength (Vacuum)	λ	1252.558 nm	[1]

TABLE XIII: $4P_{3/2} \rightarrow 5S_{1/2}$ transition properties for ^{40}K

D. $4P \rightarrow 3D$

This data is from [19]. Here the isotope shift is estimated from the normal mass shift and must be taken as approximate.

Frequency	ν	256377.08 GHz	[19]
Wavelength (Vacuum)	λ	1169.3419 nm	[1]
Transition Probability	A_{ki}	$2.20 \times 10^7 s^{-1}$	[19]
Decay Rate	$1/A_{ki}$	45.5ns	[4]
Reduced Dipole Matrix Element	$\langle i\|d\|j\rangle$	1.77×10^{-29}Cm	[2]

TABLE XIV: $4P_{1/2} \rightarrow 3D_{3/2}$ transition properties for ^{39}K

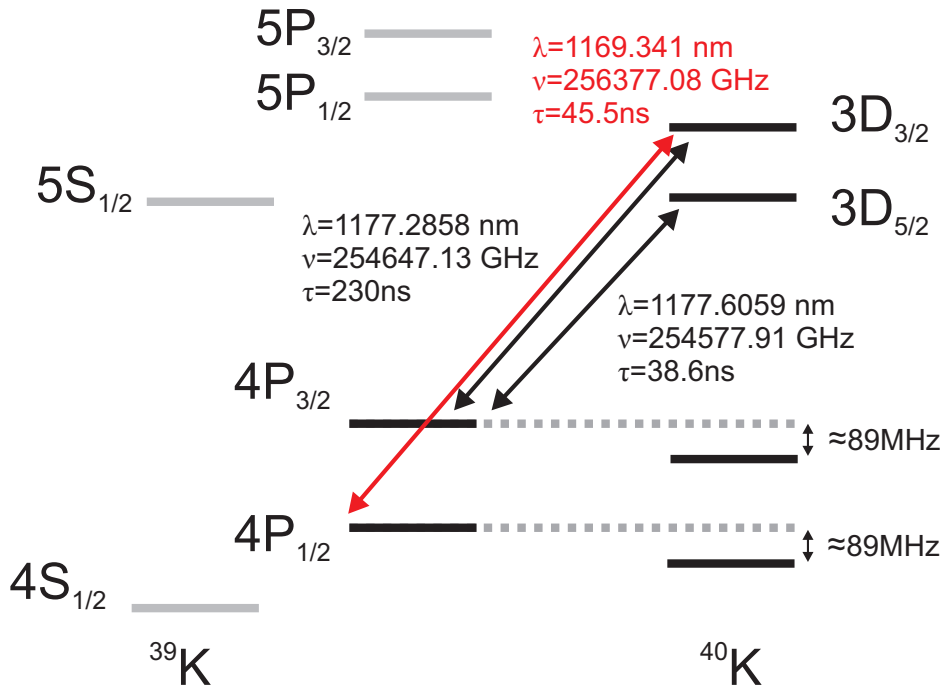

FIG. 5: $4P \rightarrow 3D$ transitions for ^{39}K with the isotope shift for ^{40}K indicated. Data from [19].

Frequency	ν	254647.13 GHz	[19]
Wavelength (Vacuum)	λ	1177.2858 nm	[1]
Transition Probability	A_{ki}	$4.34 \times 10^{6} s^{-1}$	[19]
Decay Rate	$1/A_{ki}$	230ns	[4]
Reduced Dipole Matrix Element	$\langle i\|d\|j\rangle$	7.92×10^{-30}Cm	[2]

TABLE XV: $4P_{3/2} \rightarrow 3D_{3/2}$ transition properties for ^{39}K

Frequency	ν	254577.91 GHz	[19]
Wavelength (Vacuum)	λ	1177.6059 nm	[1]
Transition Probability	A_{ki}	$2.59 \times 10^{7} s^{-1}$	[19]
Decay Rate	$1/A_{ki}$	42(3) ns	[11]
Reduced Dipole Matrix Element	$\langle i\|d\|j\rangle$	1.58×10^{-29}Cm	[2]

TABLE XVI: $4P_{3/2} \rightarrow 3D_{5/2}$ transition properties for ^{39}K

Frequency	ν	256377.17 GHz	[5]
Wavelength (Vacuum)	λ	1169.3415 nm	[1]

TABLE XVII: $4P_{1/2} \rightarrow 3D_{3/2}$ transition properties for ^{40}K

Frequency	ν	254647.22 GHz	[5]
Wavelength (Vacuum)	λ	1177.2854 nm	[1]

TABLE XVIII: $4P_{3/2} \rightarrow 3D_{3/2}$ transition properties for ^{40}K

Frequency	ν	254578.00 GHz	[5]
Wavelength (Vacuum)	λ	1177.6055 nm	[1]

TABLE XIX: $4P_{3/2} \rightarrow 3D_{5/2}$ transition properties for ^{40}K

E. $5S \rightarrow 5P$

This data is from [19]. Here the isotope shift is estimated from the normal mass shift and must be taken as approximate.

Frequency	ν	110168.56 GHz	[19]
Wavelength (Vacuum)	λ	2721.216 nm	[1]
Transition Probability	A_{ki}	$4.5 \times 10^6 s^{-1}$	[19]
Decay Rate	$1/A_{ki}$	222ns	[4]
Reduced Dipole Matrix Element	$\langle i\|d\|j\rangle$	4.01×10^{-29}Cm	[2]

TABLE XX: $5S_{1/2} \rightarrow 5P_{1/2}$ transition properties for ^{39}K

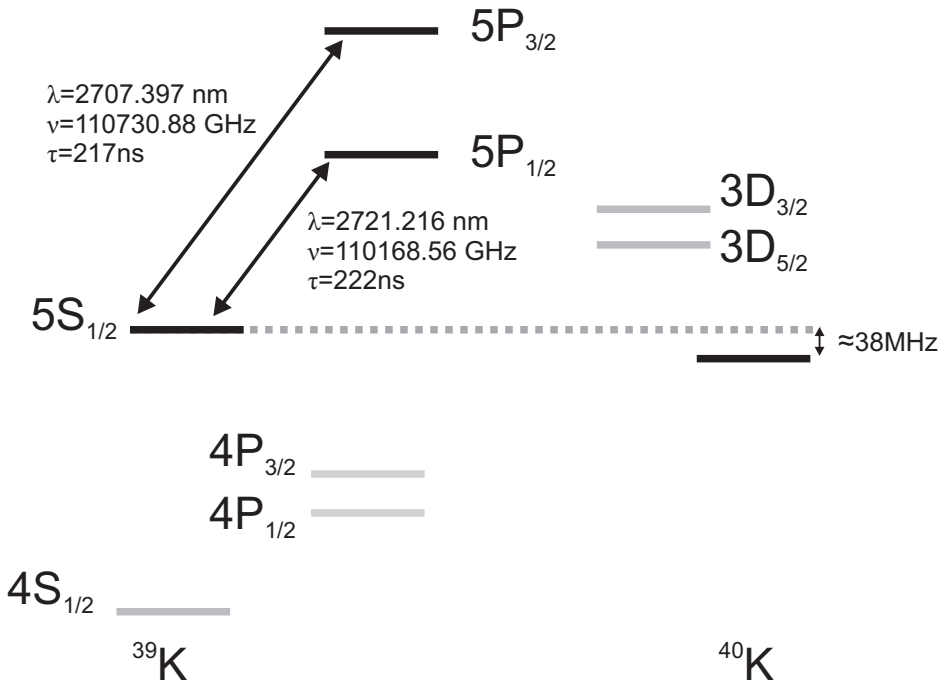

FIG. 6: $5S \rightarrow 5P$ transitions for ^{39}K with the isotope shift for ^{40}K indicated. Data from [19].

Frequency	ν	110730.88 GHz	[19]
Wavelength (Vacuum)	λ	2707.397 nm	[1]
Transition Probability	A_{ki}	$4.6 \times 10^6 s^{-1}$	[19]
Decay Rate	$1/A_{ki}$	217ns	[4]
Reduced Dipole Matrix Element	$\langle i\|d\|j\rangle$	2.85×10^{-29}Cm	[2]

TABLE XXI: $5S_{1/2} \rightarrow 5P_{3/2}$ transition properties for ^{39}K

Frequency	ν	110168.60 GHz	[5]
Wavelength (Vacuum)	λ	2721.215 nm	[1]

TABLE XXII: $5S_{1/2} \rightarrow 5P_{1/2}$ transition properties for ^{40}K

Frequency	ν	110730.92 GHz	[5]
Wavelength (Vacuum)	λ	2707.396 nm	[1]

TABLE XXIII: $5S_{1/2} \rightarrow 5P_{3/2}$ transition properties for ^{40}K

F. $3D \rightarrow 5P$

This data is from [19]. Here the isotope shift is estimated from the normal mass shift and must be taken as approximate.

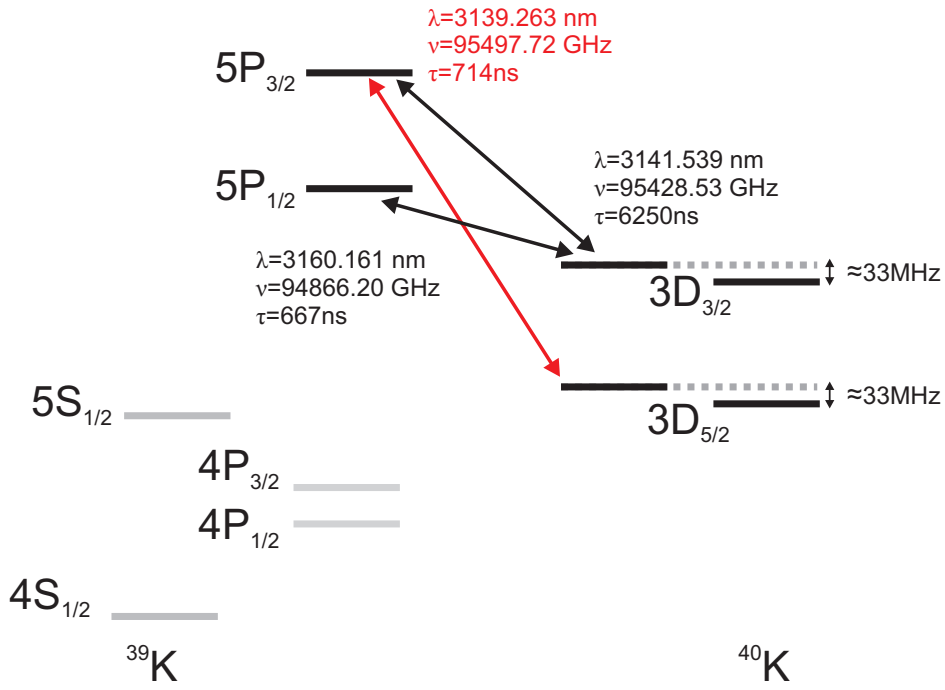

FIG. 7: $3D \rightarrow 5P$ transitions for ^{39}K with the isotope shift for ^{40}K indicated. Data from [19].

Frequency	ν	94866.20 GHz	[19]
Wavelength (Vacuum)	λ	3160.161 nm	[1]
Transition Probability	A_{ki}	$1.5 \times 10^6 s^{-1}$	[19]
Decay Rate	$1/A_{ki}$	667ns	[4]
Reduced Dipole Matrix Element	$\langle i\|d\|j\rangle$	2.90×10^{-29}Cm	[2]

TABLE XXIV: $3D_{3/2} \rightarrow 5P_{1/2}$ transition properties for ^{39}K

Frequency	ν	95428.53 GHz	[19]
Wavelength (Vacuum)	λ	3141.539 nm	[1]
Transition Probability	A_{ki}	$1.5 \times 10^5 s^{-1}$	[19]
Decay Rate	$1/A_{ki}$	6250ns	[4]
Reduced Dipole Matrix Element	$\langle i\|d\|j\rangle$	6.42×10^{-30}Cm	[2]

TABLE XXV: $3D_{3/2} \rightarrow 5P_{3/2}$ transition properties for ^{39}K

Frequency	ν	95497.72 GHz	[19]
Wavelength (Vacuum)	λ	3139.263 nm	[1]
Transition Probability	A_{ki}	$1.4 \times 10^6 s^{-1}$	[19]
Decay Rate	$1/A_{ki}$	714 ns	[11]
Reduced Dipole Matrix Element	$\langle i\|d\|j\rangle$	1.96×10^{-29}Cm	[2]

TABLE XXVI: $3D_{5/2} \rightarrow 5P_{3/2}$ transition properties for ^{39}K

Frequency	ν	94866.53 GHz	[5]
Wavelength (Vacuum)	λ	3160.150 nm	[1]

TABLE XXVII: $3D_{3/2} \rightarrow 5P_{1/2}$ transition properties for ^{40}K

Frequency	ν	95428.86 GHz	[5]
Wavelength (Vacuum)	λ	3141.528 nm	[1]

TABLE XXVIII: $3D_{3/2} \rightarrow 5P_{3/2}$ transition properties for ^{40}K

Frequency	ν	95498.01 GHz	[5]
Wavelength (Vacuum)	λ	3139.253 nm	[1]

TABLE XXIX: $3D_{5/2} \rightarrow 5P_{3/2}$ transition properties for ^{40}K

III. LEVEL STRUCTURE

In this section we will look more closely at the hyperfine structure and gyromagnetic factors (g-factors) of the individual states. We will also discuss measurements (if any) on the total lifetime of these states. These are different than the decay rates in the previous section as those referred to decay between exactly two states whereas the lifetime considers decay to all possible states.

A. $4S$ State

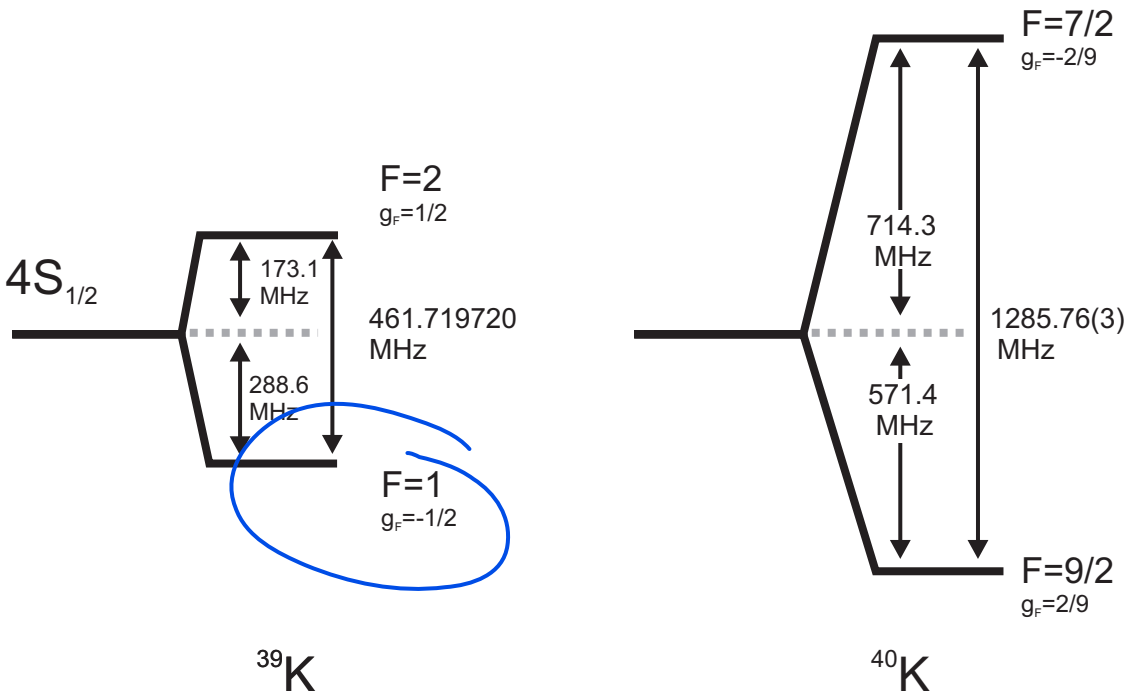

FIG. 8: $4S$ Level Structure, data from [6].

B. $4P$ State

For this state I used the hyperfine data from [10]. It should be noted that in the literature there are two sets of hyperfine constants which disagree, but there are several measurements supporting both sets. The following tables give these two sets of data.

Isotope	State	A(MHz)	B(MHz)
39	$4P_{1/2}$	27.775(42)	–
39	$4P_{3/2}$	6.093(25)	2.786(71)
40	$4P_{1/2}$	-34.523(25)	–
40	$4P_{3/2}$	-7.585(10)	-3.445(90)

TABLE XXX: $4P$ hyperfine constants from [10] and as used in Figure 9.

Isotope	State	A(MHz)	B(MHz)
39	$4P_{1/2}$	28.848(5)	–
39	$4P_{3/2}$	6.077(23)	2.875(55)

TABLE XXXI: $4P$ hyperfine constants from [9]

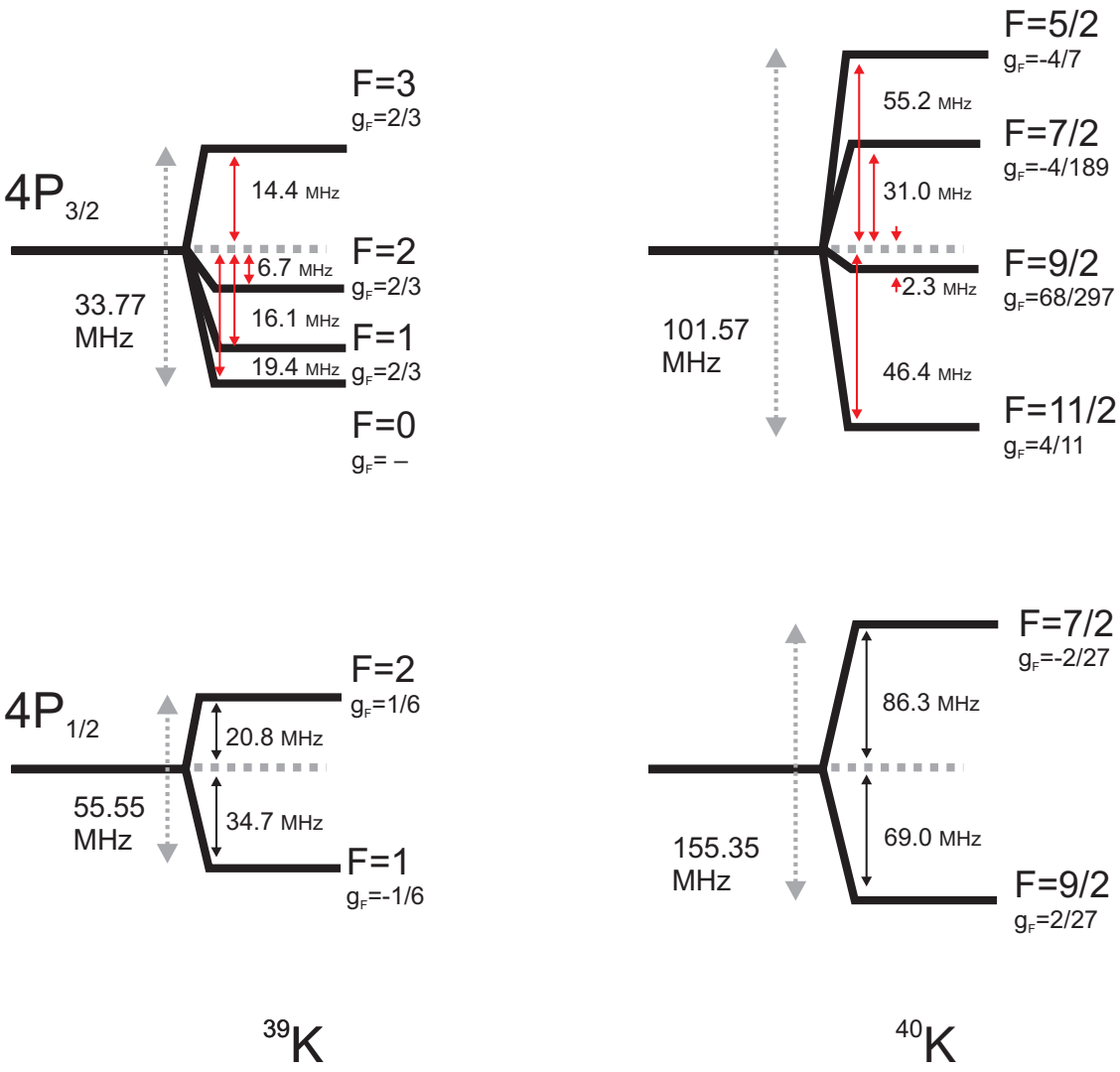

FIG. 9: $4P$ Level Structure, data from [10].

C. $5S$ State

There are few measurements of the hyperfine constants of this state in ^{39}K and none for ^{40}K . There is a theoretical lifetime measurement of $\tau = 42.5ns$ from [18].

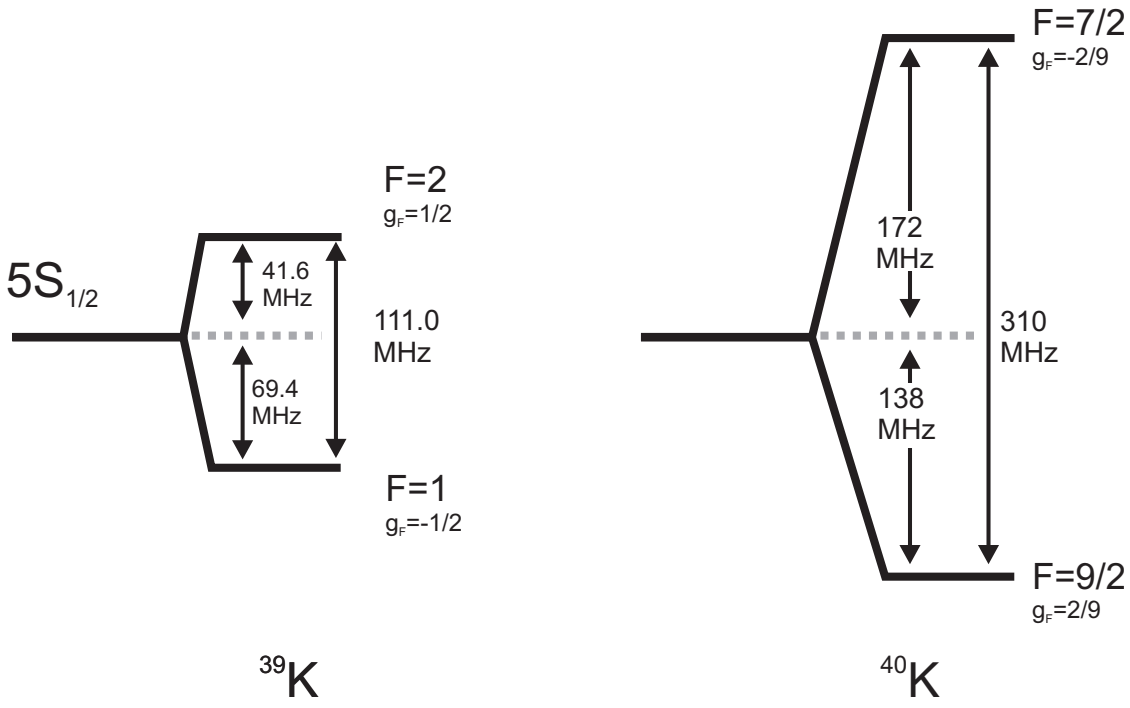

FIG. 10: $5S$ Level Structure, data from [6]. There is no experimentally measured value for ^{40}K , so these values are estimates by using the ^{39}K value multiplied by the ratio of ^{39}K to ^{40}K values for the $4S_{1/2}$ state.

D. $3D$ State

The lifetime of the $3D$ state, measured by [11], is 42(3)ns for both J levels.

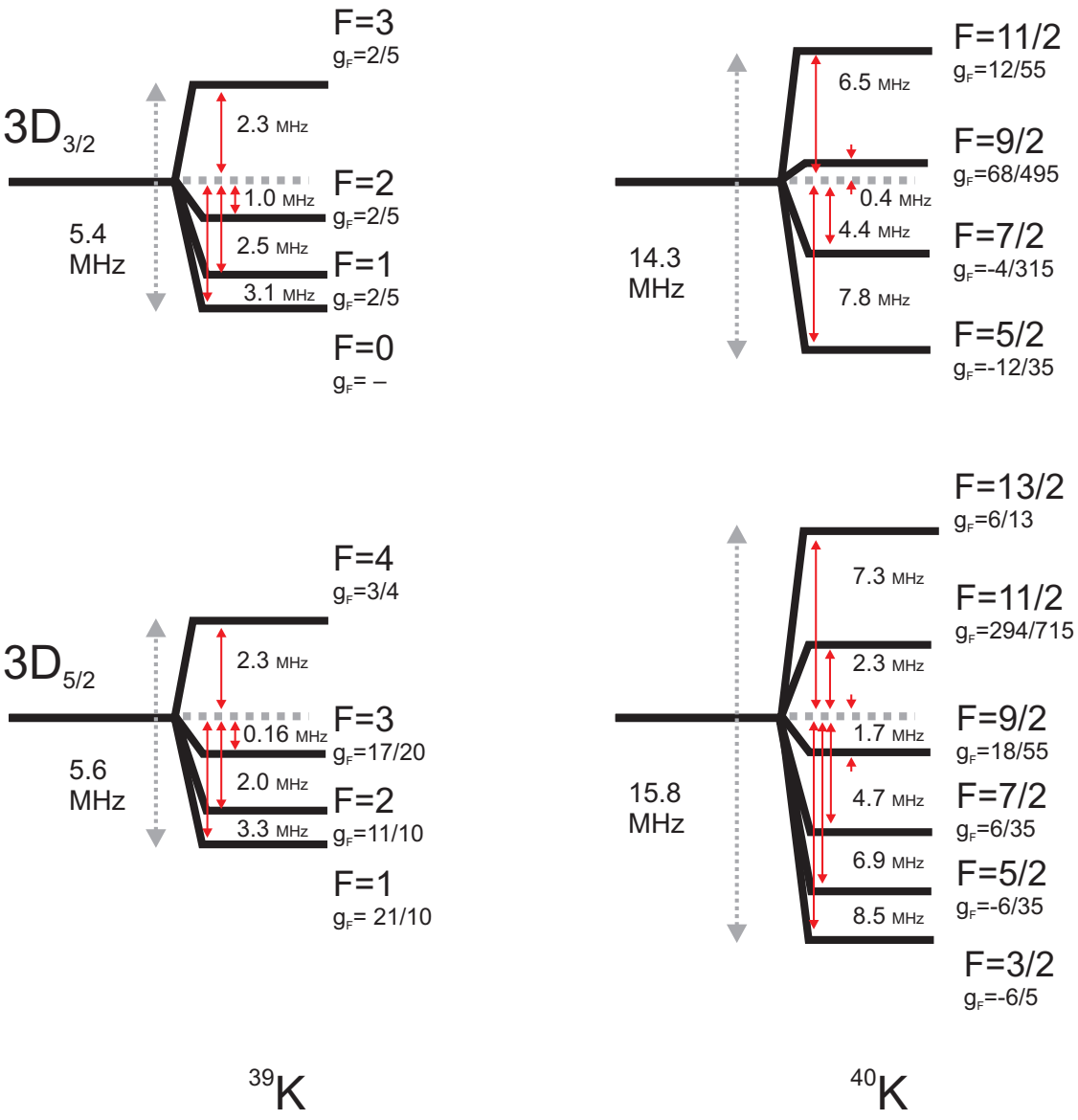

FIG. 11: $3D$ Level Structure, data from [20].

E. $5P$ State

An older measurement of the lifetime of the $5P$ state is [8], which measured $\tau = 137(2)$ns for $5P_{1/2}$ and $\tau = 134(2)$ns for $5P_{3/2}$. A more recent measurement of $5P_{1/2}$ gets $\tau = 137.6(13)$ns, [15], in agreement with [8].

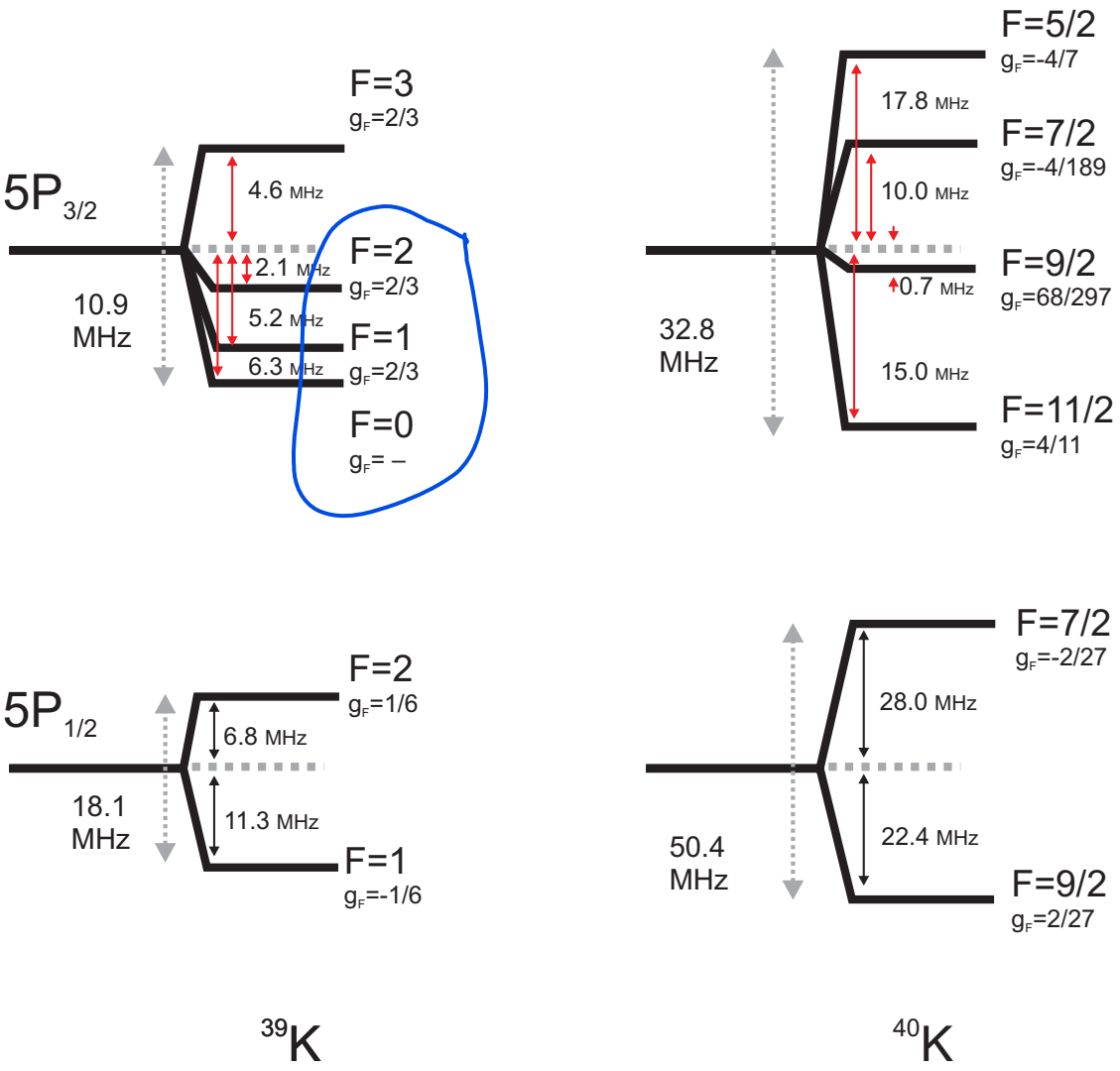

FIG. 12: $5P$ Level Structure, data from [6]. There is no measurement for A for ^{40}K in the $5P_{1/2}$ state, so it was inferred using the value for ^{39}K and the ratio of the ^{39}K to ^{40}K values for the $4P$ state.

IV. $5p$ FURTHER PROPERTIES

A. Branching Ratios for Decay

Here we will list the decay rates from the various hyperfine levels as a fraction of the total decay rate,

$$\frac{A_{FF'}}{A_{JJ'}} = (2F'+1)(2J+1)\left\{\begin{array}{ccc} J & F & I \\ F' & J' & 1 \end{array}\right\}^2$$

1. ^{39}K

J'	$F \to F'$	$\frac{A_{FF'}}{A_{JJ'}}$
3/2	$4 \to 3$	1
3/2	$3 \to 3$	1/5
3/2	$3 \to 2$	4/5
3/2	$2 \to 3$	1/50
3/2	$2 \to 2$	7/20
3/2	$2 \to 1$	63/100
3/2	$1 \to 2$	1/20
3/2	$1 \to 1$	9/20
3/2	$1 \to 0$	1/2

TABLE XXXII: Decay rate for $I = 3/2$ (^{39}K) from $J = 5/2 \to J'$

J'	$F \to F'$	$\frac{A_{FF'}}{A_{JJ'}}$	J'	$F \to F'$	$\frac{A_{FF'}}{A_{JJ'}}$	J'	$F \to F'$	$\frac{A_{FF'}}{A_{JJ'}}$
5/2	$3 \to 4$	6/7	3/2	$3 \to 3$	4/5	1/2	$3 \to 2$	1
5/2	$3 \to 3$	2/15	3/2	$3 \to 2$	1/5	1/2	$2 \to 2$	1/2
5/2	$3 \to 2$	1/105	3/2	$2 \to 3$	7/25	1/2	$2 \to 1$	1/2
5/2	$2 \to 3$	56/75	3/2	$2 \to 2$	2/5	1/2	$1 \to 2$	1/6
5/2	$2 \to 2$	7/30	3/2	$2 \to 1$	8/25	1/2	$1 \to 1$	5/6
5/2	$2 \to 1$	1/50	3/2	$1 \to 2$	8/15	1/2	$0 \to 1$	1
5/2	$1 \to 2$	7/10	3/2	$1 \to 1$	2/15			
5/2	$1 \to 1$	3/10	3/2	$1 \to 0$	1/3			
5/2	$0 \to 1$	1	3/2	$0 \to 1$	1			
			3/2	$0 \to 0$	0			

TABLE XXXIII: Decay rate for $I = 3/2$ (^{39}K) from $J = 3/2 \to J'$

J'	$F \to F'$	$\frac{A_{FF'}}{A_{JJ'}}$	J'	$F \to F'$	$\frac{A_{FF'}}{A_{JJ'}}$
3/2	$2 \to 3$	7/10	1/2	$2 \to 2$	1/2
3/2	$2 \to 2$	1/4	1/2	$2 \to 1$	1/2
3/2	$2 \to 1$	1/20	1/2	$1 \to 2$	5/6
3/2	$1 \to 2$	5/12	1/2	$1 \to 1$	1/6
3/2	$1 \to 1$	5/12			
3/2	$1 \to 0$	1/6			

TABLE XXXIV: Decay rate for $I = 3/2$ (^{39}K) from $J = 1/2 \to J'$

2. ^{40}K

J'	$F \to F'$	$\frac{A_{FF'}}{A_{JJ'}}$
3/2	$13/2 \to 11/2$	1
3/2	$11/2 \to 11/2$	16/55
3/2	$11/2 \to 9/2$	39/55
3/2	$9/2 \to 11/2$	14/275
3/2	$9/2 \to 9/2$	28/55
3/2	$9/2 \to 7/2$	11/25
3/2	$7/2 \to 9/2$	7/40
3/2	$7/2 \to 7/2$	22/35
3/2	$7/2 \to 5/2$	11/56
3/2	$5/2 \to 7/2$	3/7
3/2	$5/2 \to 5/2$	4/7
3/2	$3/2 \to 5/2$	1

TABLE XXXV: Decay rate for $I = 4$ (^{40}K) from $J = 5/2 \to J'$

J'	$F \to F'$	$\frac{A_{FF'}}{A_{JJ'}}$	J'	$F \to F'$	$\frac{A_{FF'}}{A_{JJ'}}$	J'	$F \to F'$	$\frac{A_{FF'}}{A_{JJ'}}$
5/2	$11/2 \to 13/2$	7/9	3/2	$11/2 \to 11/2$	39/55	1/2	$11/2 \to 9/2$	1
5/2	$11/2 \to 11/2$	32/165	3/2	$11/2 \to 9/2$	16/55	1/2	$9/2 \to 9/2$	16/27
5/2	$11/2 \to 9/2$	14/495	3/2	$9/2 \to 11/2$	96/275	1/2	$9/2 \to 7/2$	11/27
5/2	$9/2 \to 11/2$	156/275	3/2	$9/2 \to 9/2$	289/1485	1/2	$7/2 \to 9/2$	7/27
5/2	$9/2 \to 9/2$	56/165	3/2	$9/2 \to 7/2$	308/675	1/2	$7/2 \to 7/2$	20/27
5/2	$9/2 \to 7/2$	7/75	3/2	$7/2 \to 9/2$	77/135	1/2	$5/2 \to 7/2$	1
5/2	$7/2 \to 9/2$	11/30	3/2	$7/2 \to 7/2$	1/945			
5/2	$7/2 \to 7/2$	44/105	3/2	$7/2 \to 5/2$	3/7			
5/2	$7/2 \to 5/2$	3/14	3/2	$5/2 \to 7/2$	4/7			
5/2	$5/2 \to 7/2$	11/63	3/2	$5/2 \to 5/2$	3/7			
5/2	$5/2 \to 5/2$	8/21						
5/2	$5/2 \to 3/2$	4/9						

TABLE XXXVI: Decay rate for $I = 4$ (^{40}K) from $J = 3/2 \to J'$

J'	$F \to F'$	$\frac{A_{FF'}}{A_{JJ'}}$	J'	$F \to F'$	$\frac{A_{FF'}}{A_{JJ'}}$
3/2	$9/2 \to 11/2$	3/5	$1/2 \to 1/2$	$9/2 \to 9/2$	11/27
3/2	$9/2 \to 9/2$	8/27	$1/2 \to 1/2$	$9/2 \to 7/2$	16/27
3/2	$9/2 \to 7/2$	14/135	$1/2 \to 1/2$	$7/2 \to 9/2$	20/27
3/2	$7/2 \to 9/2$	55/216	$1/2 \to 1/2$	$7/2 \to 7/2$	7/27
3/2	$7/2 \to 7/2$	10/27			
3/2	$7/2 \to 5/2$	3/8			

TABLE XXXVII: Decay rate for $I = 4$ (^{40}K) from $J = 1/2 \to J'$

3. Branching Ratio from $5P_{J=3/2,F=11/2}$ for ^{40}K

In this section we will calculate the branching ratio between decay into the $F = 9/2$ versus the $F = 7/2$ ground state of ^{40}K ($4S_{1/2}$) assuming the atom starts in the state $5P_{J=3/2,F=11/2}$. This will allow us to get an idea of the number of scattering events before a repump photon is required. To calculate the ratio of total scattering events that end up in a certain state we must sum over all the paths that lead to that state. The relative probability of a path is obtained by multiplying by the branching ratio each time there is a choice between paths. These branching ratios are illustrated in Figure 13.

Summing all the paths that go to $F = 9/2$ (multplying by the branching ratios at each step) we get that there is an $\approx 80\%$ chance of decaying to the $F = 9/2$ state, which means that 1 out of every 5 scattering events leads to an atom which must be repumped.

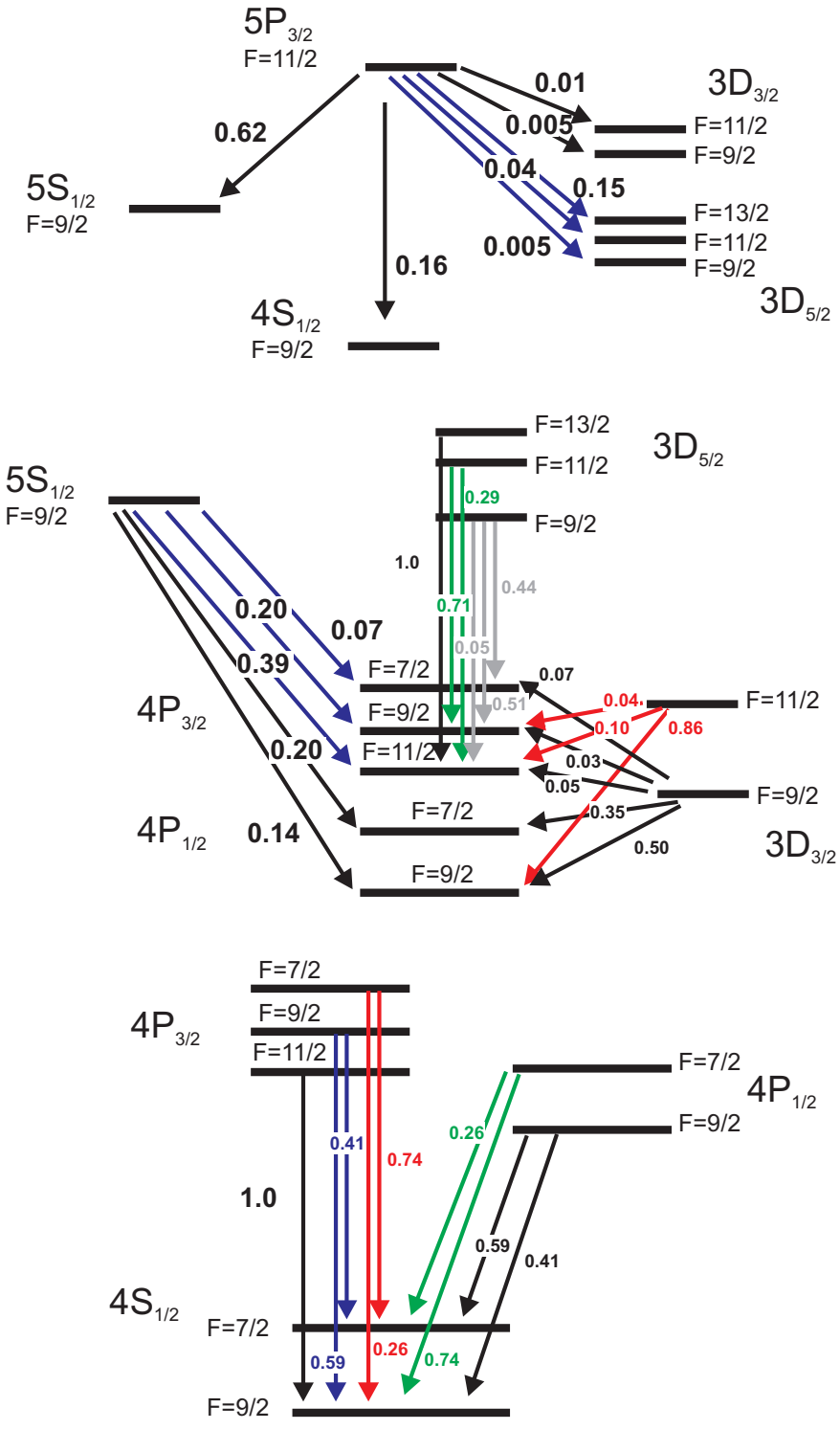

FIG. 13: Branching ratios for paths from $5P_{J=3/2,F=11/2} \rightarrow 4S$

B. Absorption Cross-Section and Saturation Intensity

Here we will calculate the absorption cross-section for the $5P$ transition and the saturation intensity. Typically these quantities are defined for cycling transitions where the cross-section is defined as,

$$\sigma = \frac{3\lambda^2}{2\pi}$$

and the saturation intensity is defined as,

$$I_{sat} = \frac{\hbar\omega_0^3\Gamma}{12\pi c^2}$$

where the saturation itensity is the intensity required to put 1/4 of the atoms in the excited state on resonance. However, for driving on the $5P$ transition we have no cycling transition and we cannot define an effective two-state system. In fact as we saw in the last section, we cannot achieve steady-state with one beam since we drive ourselves into a dark ground state after approximately five scattering events. However, we can make the assumption that all we see is the J structure and then we can try and define a multi-level cross-section and saturation intensity.

1. Three-Level Approximation

The first approximation we can use is to assume that the limiting transition is out of the $5P$ state and then we get that we can use the two-state result that,

$$\rho_{22} = \frac{1}{2}\frac{I/I_{sat}}{1+4\left(\Delta/\Gamma\right)^2+I/I_{sat}}$$

where

$$I_{sat} = \frac{I\Gamma^2}{2\Omega^2}$$

However, Γ is the total decay from the $5P$ state and

$$\frac{\Omega^2}{I} = \left(\frac{2\pi c^2 \Gamma_0}{\hbar \omega_0^3}\right)$$

where Γ_0 is the decay just along the $5P \rightarrow 4S$ transition. Note that here I have used the unpolarized Rabi rate since driving with polarized light would make the assumption of ignoring hyperfine states invalid. Therefore,

$$\begin{aligned} I_{sat} &= \frac{\Gamma^2}{2} \frac{\hbar \omega_0^3}{2\pi c^2 \Gamma_0} \\ &= \frac{\hbar \omega_0^3 \Gamma^2}{4\pi c^2 \Gamma_0} \end{aligned}$$

which is $\approx 43\text{mW/cm}^2$ (compared to $\approx 4.5\text{mW/cm}^2$ for unpolarized light on the D lines). For the cross-section,

$$\begin{aligned} \sigma &= \frac{\hbar \omega_0 \Gamma}{2 I_{sat}} \\ &= \frac{\hbar \omega_0 \Gamma}{2} \frac{4\pi c^2 \Gamma_0}{\hbar \omega_0 \omega_0^2 \Gamma} \\ &= \frac{2\pi c^2}{\omega_0^2} \frac{\Gamma_0}{\Gamma} \\ &= \frac{\lambda^2}{2\pi} \frac{\Gamma_0}{\Gamma} \end{aligned}$$

which is $\approx 0.0042 \mu\text{m}^2$. Compared to $\approx 0.094 \mu\text{m}^2$ for the D line transitions, this means the $4S \rightarrow 5P$ cross-section is ≈ 20 times smaller.

2. Including all Levels

In this solution we use all the levels as shown in Figure 1. Letting,

$$\Gamma = \left(\Gamma_{5P \rightarrow 4S} + \Gamma_{5P \rightarrow 5S} + \Gamma_{5P \rightarrow 3D_{3/2}} + \Gamma_{5P \rightarrow 3D_{5/2}}\right)$$

The optical Bloch equations are (where 1 is $4S$ and 2 is $5P$ and all the other states are labeled accordingly),

$$
\begin{aligned}
\dot{\rho}_{22} &= \frac{i\Omega}{2}\rho_{21} - \frac{i\Omega^*}{2}\rho_{12} - \Gamma\rho_{22} \\
\dot{\rho}_{21} &= i\Delta\rho_{21} - \frac{i\Omega^*}{2}(\rho_{11} - \rho_{22}) - \frac{\Gamma}{2}\rho_{21} \\
\dot{\rho}_{5S} &= \Gamma_{5P\to 5S}\rho_{22} - (\Gamma_{5S\to 4P_{3/2}} + \Gamma_{5S\to 4P_{1/2}})\rho_{5S} \\
\dot{\rho}_{3D_{3/2}} &= \Gamma_{5P\to 3D_{3/2}}\rho_{22} - (\Gamma_{3D_{3/2}\to 4P_{3/2}} + \Gamma_{3D_{3/2}\to 4P_{1/2}})\rho_{3D_{3/2}} \\
\dot{\rho}_{3D_{5/2}} &= \Gamma_{5P\to 3D_{5/2}}\rho_{22} - \Gamma_{3D_{5/2}\to 4P_{3/2}}\rho_{3D_{5/2}} \\
\dot{\rho}_{4P_{3/2}} &= \Gamma_{5S\to 4P_{3/2}}\rho_{5S} + \Gamma_{3D_{3/2}\to 4P_{3/2}}\rho_{3D_{3/2}} + \Gamma_{3D_{5/2}\to 4P_{3/2}}\rho_{3D_{5/2}} - \Gamma_{4P_{3/2}\to 4S}\rho_{4P_{3/2}} \\
\dot{\rho}_{4P_{1/2}} &= \Gamma_{5S\to 4P_{1/2}}\rho_{5S} + \Gamma_{3D_{3/2}\to 4P_{1/2}}\rho_{3D_{3/2}} - \Gamma_{4P_{1/2}\to 4S}\rho_{4P_{1/2}} \\
1 &= \rho_{22} + \rho_{11} + \rho_{5S} + \rho_{3D_{3/2}} + \rho_{3D_{5/2}} + \rho_{4P_{1/2}} + \rho_{4P_{3/2}}
\end{aligned}
$$

The steady-state solutions are,

$$
\begin{aligned}
\frac{\rho_{22}}{\rho_{5S}} &= \frac{\Gamma_{5S\to 4P_{3/2}} + \Gamma_{5S\to 4P_{1/2}}}{\Gamma_{5P\to 5S}} = 5.11 \\
\frac{\rho_{22}}{\rho_{3D_{3/2}}} &= \frac{\Gamma_{3D_{3/2}\to 4P_{3/2}} + \Gamma_{3D_{3/2}\to 4P_{1/2}}}{\Gamma_{5P\to 3D_{3/2}}} = 176 \\
\frac{\rho_{22}}{\rho_{3D_{5/2}}} &= \frac{\Gamma_{3D_{5/2}\to 4P_{3/2}}}{\Gamma_{5P\to 3D_{5/2}}} = 18.5 \\
\frac{\rho_{22}}{\rho_{4P_{3/2}}} &= \frac{\Gamma_{4P_{3/2}\to 4S}}{\Gamma_{5S\to 4P_{3/2}}/5.11 + \Gamma_{3D_{3/2}\to 4P_{3/2}}/176 + \Gamma_{3D_{5/2}\to 4P_{3/2}}/18.5} = 8.5 \\
\frac{\rho_{22}}{\rho_{4P_{1/2}}} &= \frac{\Gamma_{4P_{1/2}\to 4S}}{\Gamma_{5S\to 4P_{1/2}}/5.11 + \Gamma_{3D_{3/2}\to 4P_{1/2}}/176} = 22.4
\end{aligned}
$$

Therefore,

$$
\begin{aligned}
\rho_{11} &= 1 - 1.42\rho_{22} \\
&= 1 - \alpha\rho_{22}
\end{aligned}
$$

If we write ρ_{22} in terms of α,

$$
\rho_{22} = \frac{\Omega^2}{\Gamma^2 + 4\Delta^2 + (1+\alpha)\Omega^2}
$$

So we see that our cross-section from the previous section was correct. However, the saturation intensity will be a little different. If we use the saturation intensity definition as the intensity required to put 1/4 of the atoms in the excited state then,

$$I_{sat} = \frac{\hbar\omega_0^3\Gamma^2}{2\pi c^2\Gamma_0}\frac{1}{3-\alpha}$$

Since $\alpha = 1.42$ we underestimated I_{sat} by $\approx 25\%$ with the three-level approximation. This calculation also tells us that $\approx 40\%$ of the atoms in the excited state are in the intermediate states (ie. if 10% of the atoms are in the excited state, 4% are in the intermediate states and 86% are in the ground state).

[1] Wavelength obtained as c/ν where c is the value from [16].

[2] Calculated using Equation 1.

[3] Frequency obtained as c/λ where c is the value from [16].

[4] τ obtained from $1/A_{ki}$.

[5] This value is obtained by estimating the isotope shift from the normal mass shift.

[6] E. Arimondo, M. Inguscio, and P. Violino. Experimental determinations of the hyperfine structure in the alkali atoms. *Rev. Mod. Phys.*, 49(1):31–75, Jan 1977.

[7] N Bendali, H T Duong, and J L Vialle. High-resolution laser spectroscopy on the d1 and d2 lines of 39,40,441k using rf modulated laser light. *Journal of Physics B: Atomic and Molecular Physics*, 14(22):4231–4240, 1981.

[8] R. W. Berends, W. Kedzierski, J. B. Atkinson, and L. Krause. The radiative lifetimes of the potassium 5p, 6p and 7p states. *Spectrochimica Acta Part B: Atomic Spectroscopy*, 43(9-11):1069 – 1073, 1988.

[9] Dipankar Das and Vasant Natarajan. High-precision measurement of hyperfine structure in the d lines of alkali atoms. *J. Phys. B*, 41(3):035001 (12pp), 2008.

[10] Stephan Falke, Eberhard Tiemann, Christian Lisdat, Harald Schnatz, and Gesine Grosche. Transition frequencies of the d lines of [sup 39]k, [sup 40]k, and [sup 41]k measured with a femtosecond laser frequency comb. *Phys. Rev. A*, 74(3):032503, 2006.

[11] D J Hart and J B Atkinson. Lifetimes of some excited s and d states of potassium. *J. Phys. B*, 19(1):43–49, 1986.

[12] Robert S. Williamson III. *Magneto-Optical Trapping of Potassium Isotopes.* PhD thesis, University of Wisconsin - Madison, 1997.

[13] L.D. Landau and E.M. Lifshitz. *Quantum Mechanics: Non-Relativistic Theory.* Pergamon Press, 1977.

[14] Lindsay LeBlanc. The hyperfine structure of potassium-40. Technical report, University of Toronto, 2006.

[15] A. Mills, J. A. Behr, L. A. Courneyea, and M. R. Pearson. Lifetime of the potassium 5p1?2 state. *Phys. Rev. A*, 72(2):024501, Aug 2005.

[16] P.J. Mohr, B.N. Taylor, and D.B. Newell. The 2006 CODATA recommended values of the

fundamental physical constants, web version 5.1. Online, http://physics.nist.gov/constants, May 2009.

[17] Yu Ralchenko, A.E. Kramida, J. Reader, and NIST ASD Team. NIST Atomic Spectra Database (version 3.1.5). Online, http://physics.nist.gov/asd3, May 2009.

[18] U. I. Safronova and M. S. Safronova. High-accuracy calculation of energies, lifetimes, hyperfine constants, multipole polarizabilities, and blackbody radiation shift in [sup 39]k. *Physical Review A (Atomic, Molecular, and Optical Physics)*, 78(5):052504, 2008.

[19] J. E. Sansonetti. Wavelengths, transition probabilities, and energy levels for the spectra of potassium (k i through k xix). *Journal of Physical and Chemical Reference Data*, 37(1):7–96, 2008.

[20] A. Sieradzan, R. Stoleru, Wo Yei, and M. D. Havey. Measurement of hyperfine coupling constants in the $3dt2dj$ levels of $k39$, $k40$, and $k41$ by polarization quantum-beat spectroscopy. *Phys. Rev. A*, 55(5):3475–3483, May 1997.

[21] Daniel Steck, 2001. Rubidium 87 D Line Data.

[22] H. Wang, J. Li, X. T. Wang, C. J. Williams, P. L. Gould, and W. C. Stwalley. Precise determination of the dipole matrix element and radiative lifetime of the $k39$ 4p state by photoassociative spectroscopy. *Phys. Rev. A*, 55(3):R1569–R1572, Mar 1997.